

Measuring the Phase Portrait of an Ion Beam in a Tandem Accelerator with Vacuum Insulation

M. I. Bikchurina^{a,b}, T. A. Bykov^{a,b}, Ya. A. Kolesnikov^{a,b,*}, A. N. Makarov^{a,b}, G. M. Ostreinov^{a,b},
S. S. Savinov^{a,b}, S. Yu. Taskaev^{a,b}, and I. M. Shchudlo^{a,b}

^a Budker Institute of Nuclear Physics, Siberian Branch, Russian Academy of Sciences,
Novosibirsk, 630090 Russia

^b Novosibirsk State University, Novosibirsk, 630090 Russia

*e-mail: Ya.A.Kolesnikov@inp.nsk.su

Received March 10, 2022; revised March 16, 2022; accepted March 19, 2022

Abstract—One of the charged-particle accelerators with relatively low energy and relatively high current is the vacuum-insulated tandem accelerator proposed for boron neutron capture therapy and planned for use in a number of other applications requiring a more remote location of the neutron-generating target from the accelerator. In this work, the phase portrait of the ion beam and its dependence on the ion beam current and the strength of the magnetic lens focusing the beam of negative hydrogen ions on the input of the accelerator are measured. It is shown that the modernization of the magnetic lens contributed to the reduction of the spherical aberration of the lens and improved the quality of the negative ion beam. It has been established that the ion beam emittance increases with increasing current, and the space charge affects the phase portrait of the ion beam in the low energy transport path. To compensate for the action of the space charge on the phase portrait of the proton beam, the strength of the magnetic lens is changed. The obtained experimental data indicate that the proton beam can be transported to the site of the planned location of the neutron-generating target without adding focusing elements.

DOI: 10.1134/S0020441222040169

1. INTRODUCTION

A tandem electrostatic accelerator of charged particles of an original design, a Vacuum-Insulated Tandem Accelerator (VITA), has been proposed and created at the Budker Institute of Nuclear Physics of the Siberian Branch of the Russian Academy of Sciences. The accelerator produces a beam of protons with an energy that can vary within 0.6–2.3 MeV with high stability and a monochromaticity of 0.1%. The beam current varies over a wide range, from 1 nA to 10 mA, with a stability of 0.4%. The accelerator is used to develop the technique of boron neutron capture therapy [1, 2], including equipping it with a neutron source supplied in Xiamen (China) and neutron sources manufactured for Pavia (Italy) and Moscow (Russia). The accelerator is also used to study radiation blistering of metals [3, 4], perform activation analysis of materials [5], obtain fundamental knowledge about the reaction cross section [6], and for other applications. In the near future, the facility is planned to be used for radiation testing of materials with fast neutrons and for testing the methodology of boron neutron capture therapy on large domestic animals with spontaneous tumors. These studies require the placement of a neutron-generating target at a greater

distance from the accelerator than in previous applications.

The need to transport a proton beam over long distances has made it important to measure the phase portrait of a proton beam in order to determine whether additional focusing elements are required for its transportation. To implement the stated problem, it is necessary to measure the phase portrait of the ion beam and study its dependence on the ion current and the strength of the magnetic lens focusing the ion beam at the entrance to the accelerator.

2. EXPERIMENTAL FACILITY

Figure 1 shows a diagram of the experimental facility. A stationary proton beam is produced in a Vacuum-Insulated Tandem Accelerator (VITA). The term “tandem” means that the applied accelerating voltage is used twice. Negative hydrogen ions are injected into the input of the tandem accelerator, accelerated by a positive potential applied to the central electrode, then stripped to positive ions and accelerated again by the same potential. The accelerator has a special design, which, unlike conventional tandem accelerators, does not use accelerating tubes. Instead, nested intermedi-

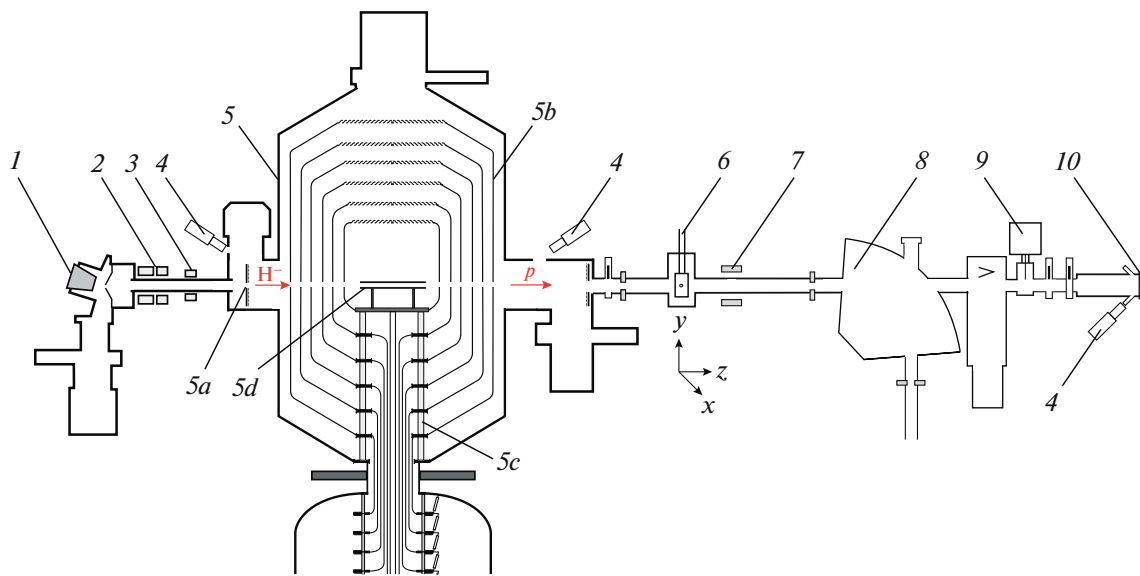


Fig. 1. Scheme of the experimental facility. 1—Source of negative ions; 2—magnetic lens; 3—corrector; 4—video cameras; 5—tandem accelerator with vacuum insulation (5a—inlet hole; 5b—intermediate- and high-voltage electrodes; 5c—feedthrough insulator; 5d—gas-stripping target); 6—cooled diaphragm; 7—noncontact current sensor; 8—bending magnet; 9—wire scanner; 10—lithium target.

ate electrodes $5b$ fixed on the feedthrough insulator $5c$, as shown in Fig. 1, are used. This design of the electrodes makes it possible to provide a high rate of ion acceleration, up to 25 kV/cm, but the electrostatic lens at the accelerator input is strong. For this reason, the injected beam of negative hydrogen ions is refocused on the inlet $5a$ magnetic lens accelerator 2.

We previously found [7] that the transport of a beam of negative hydrogen ions from an ion source 1 to the accelerator 5 is affected by the space charge and spherical aberration of the magnetic lens 2, representing two identical coils at some distance from each other. After this fact was clarified, the magnetic lens was modernized: the coil closest to the ion source was

strengthened and brought closer to the source, and the second coil was placed close to the first one. The aim of the study was to find out how much the modernization carried out reduced the spherical aberration of the lens and improved the quality of the ion beam.

If the phase portrait of a beam of negative hydrogen ions was previously measured with a movable diaphragm and an OWS-30 wire scanner (D-Pace, Canada) [8], now it is measured with an ES-4 emittance scanner (D-Pace, Canada) [9], adequately suitable for this task. The emittance scanner is installed at a distance of 57 mm in front of the entrance aperture $5a$ accelerator; the entrance slit of the scanner is 0.1 mm;

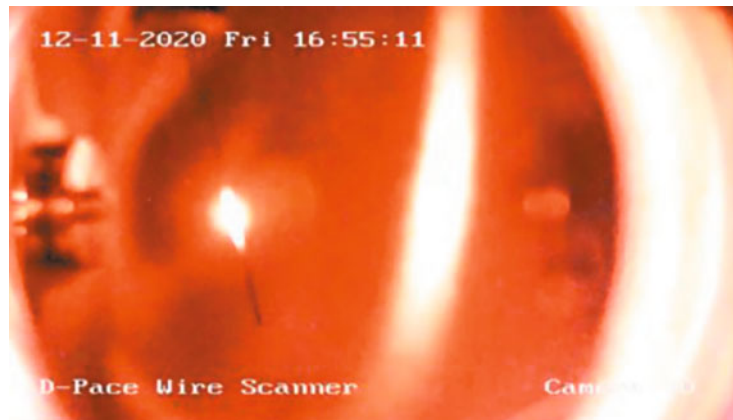


Fig. 2. Photograph of a scanner wire crossing a proton beam at a proton beam current of 3 mA.

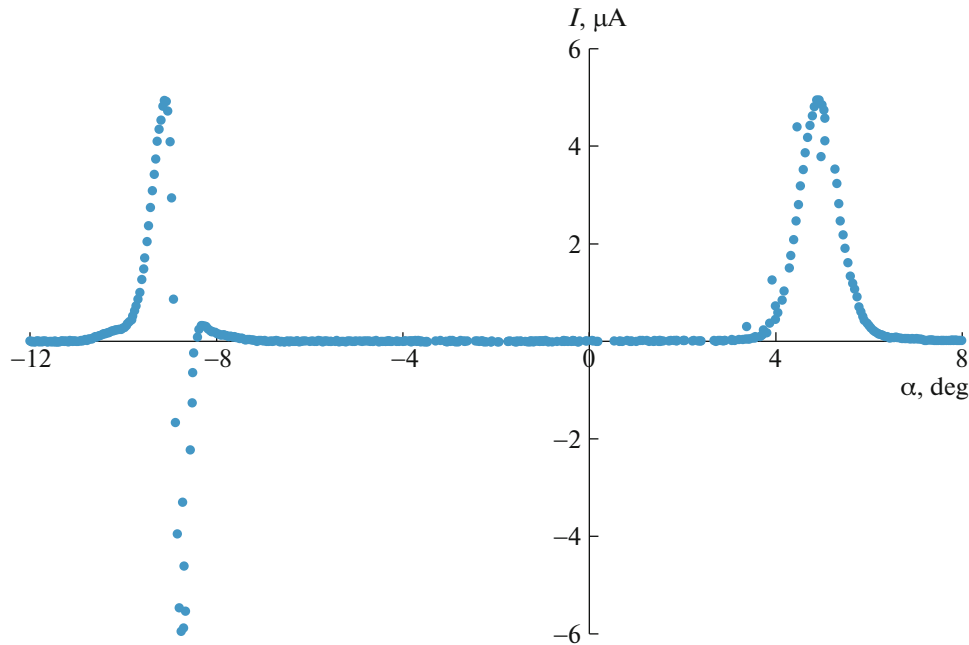


Fig. 3. Oscillogram of the scanner signal at a proton beam current of 3 mA.

measurements were performed with a step of 0.1 mm and 1 mrad.

We used a methodical technique with a movable diaphragm and a wire scanner to measure the phase portrait of a proton beam. In this method, a part of the ion beam is cut out with a diaphragm, and its profile is measured at a certain distance with a wire scanner. The set of data obtained by scanning the ion beam with a diaphragm makes it possible to reconstruct the phase portrait of the ion beam and determine its emittance.

Cooled diaphragm 6 installed at a distance of 1.86 m from the center of the accelerator. The diaphragm is a copper rectangular parallelepiped with 64×64 -mm sides, 16 mm thick. A hole with a diameter of 1 mm was drilled in the center of the diaphragm and countersinking with a diameter of 10 mm was made on both sides. Channels 10 mm in diameter are made inside the diaphragm to cool it with water. Cooling water is supplied to the diaphragm and removed from it through metal tubes soldered into the diaphragm. By means of metal tubes, the diaphragm is fixed to a TTX100-100-200-YZS 3D movable motion input (UHV Design), with which it can be controlled in a plane orthogonal to the direction of propagation of the proton beam.

The transverse profile of the proton beam is measured with an OWS-30 wire scanner (D-Pace, Canada) (9) [8], installed after the bending magnet at a distance of 3.11 m from the diaphragm 6. The scanner consists of two 0.5-mm in diameter and 49-mm long tungsten wires, fixed on a common rod, which is deflected at an angle of 13.5° from the axis crossing the

center of the ion beam. When measuring, the rod rotates to an angle of -13.5° and comes back. The axis of rotation of the rod is located at a distance of 190 mm from the center of the ion beam. When crossing the center of the proton beam each of the wires is inclined at an angle of 45° to the plane of the scanner flange. Since the scanner is placed at an angle of 45° to the horizontal, one of the wires crosses the proton beam vertically, the other horizontally. When the rod moves, the current falling on this wire and the angle of deflection of the rod are measured. The values obtained for

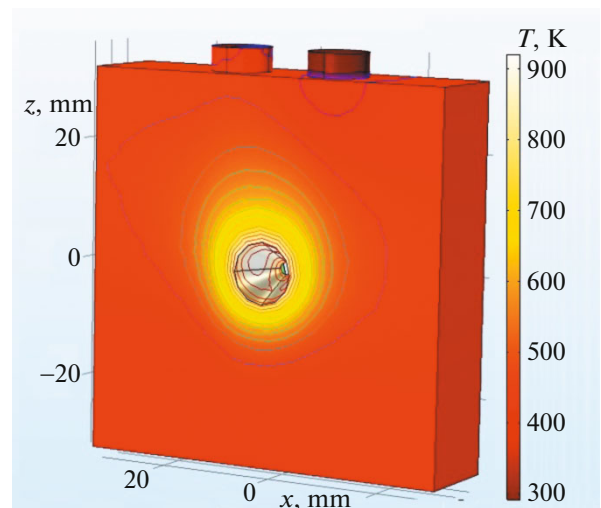


Fig. 4. Simulation of diaphragm heating when it is placed in the center of a proton beam with a current of 3 mA.

Table 1. Results of Measurements of the Phase Portrait of a Beam of Negative Hydrogen Ions with an energy of 22 keV

Current, mA	y , mm	y' , mrad	ϵ_{norm} , mm mrad
0.44	3.92	31.8	0.13
0.7	4.31	31	0.14
0.85	4.36	30.5	0.14
1	4.45	30.1	0.15
1.5	4.40	26.9	0.17
2	4.54	25.7	0.18
3	4.59	29.5	0.20

a beam diameter of less than 30 mm make it possible to reconstruct the transverse profile of the proton beam with a spatial resolution of 0.1 mm.

To correctly measure the proton current, a modernization was carried out: in front of the scanner and behind it, at a distance of 50 mm, a metal ring with an inner diameter of 60 mm was installed, each of which was under a negative potential of 300 V to suppress the secondary emission of electrons from the scanner wires.

The characteristic values of the current to the scanner wire were 10^{-6} A, picoammeter error was 10^{-10} A. Since there are two wires that intersect the center of the beam at angles different by 90° and cannot be in the beam at the same time, measurements made by the scanner make it possible to obtain profiles of the proton beam in two perpendicular directions in a plane orthogonal to the beam. Placing the scanner axis at an angle of 45° to the axes x and y makes it possible to reconstruct the phase portrait of the beam in the space of coordinates and propagation angles (x, x') and (y, y') .

The documentation for the wire scanner instructs that the maximum energy of the measured beam should not exceed 1 MeV, and the beam power density should not exceed 1 W/mm^2 . We used the scanner in a mode not provided by the manufacturer, namely with higher energy and higher power density. It has been established that the scanner provides reliable measurements with the required spatial resolution at a proton energy of 2 MeV and a current of up to 3 mA. At a current of 3 mA, as seen in Fig. 2, the scanner wire crossing the proton beam is heated to such an extent that it initiates a breakdown in the vacuum gap between the heated wire and metal rings under a negative potential of 300 V. Figure 3 shows the oscillogram of the scanner signal, according to which, during the reverse passage of the wire through the proton beam the signal became negative instead of positive due to the formation of plasma and shorting of the gap between the scanner wire and the ring under a negative potential.

The strong heating of the cooled diaphragm, which reduces the electric strength of the accelerator due to the enhanced emission of electrons from its surface, also leads to a limitation of the proton beam current to 3 mA. Thus, at a proton beam current of 3 mA and a diaphragm placed in the center of the beam, the countersink area, as shown by the simulation performed in the Comsol Multiphysics program, heats up to 900 K (Fig. 4) and, like a flashlight, illuminates the output diaphragm of the accelerator (Fig. 5).

Finishing the description of the experiment, we point out that the position and size of the ion beam in the accelerator is controlled by pairs of video cameras (4 in Fig. 1), pointing at the input and output diaphragms of the external accelerating electrode. The proton beam current is measured with a noncontact current sensor NPCT (Bergoz, France) (7 in Fig. 1). A beam of protons is taken on a lithium target (10 in Fig. 1), using it as a Faraday cup to measure the proton beam current and to control the position and size of the beam on the lithium surface by luminescence recorded by a video camera 4 [10].

Note that the position and size of the beam in front of the accelerator inlet is usually controlled by a wire scanner. This control is important for optimal ion acceleration and further transport of the proton beam, but this diagnostic was not used in this study because either an emittance scanner was installed instead of a wire scanner or a wire scanner was used to measure the phase portrait of the proton beam.

3. MEASUREMENT RESULTS AND THEIR DISCUSSION

The phase portrait of a beam of negative hydrogen ions was measured by us earlier using a diaphragm and a wire scanner, and the results were published in [7]. The effect of the spherical aberration of the magnetic lens was clearly visible on the phase profile of the ion beam, and the normalized emittance was determined as 1.7 mm mrad (this value was understood here as the area of the ellipse, inside which $2/3$ of the ion beam current is concentrated).

Let us refine the concept of “emitter” for an unambiguous understanding of the results obtained. This term is used to describe the beam size in phase spaces (x, x') or (y, y') .

Emittance in phase space (x, x') is defined as $\epsilon_{xx'} = \epsilon_{\text{rms}} = (\det(\sigma_{xx'}))^{1/2}$, where $\sigma_{xx'} = \begin{bmatrix} \langle x^2 \rangle & \langle xx' \rangle \\ \langle xx' \rangle & \langle x'^2 \rangle \end{bmatrix}$; $x^2 = \frac{1}{N} \sum_1^N x_i^2$; $\langle x'^2 \rangle = \frac{1}{N} \sum_1^N x_i'^2$; $\langle xx' \rangle = \frac{1}{N} \sum_1^N x_i x_i'$. The area of the phase portrait ellipse is defined as $S = \pi \epsilon_{xx'}$.

The emittance of a finite beam with a uniform charge distribution in the phase space is well defined.

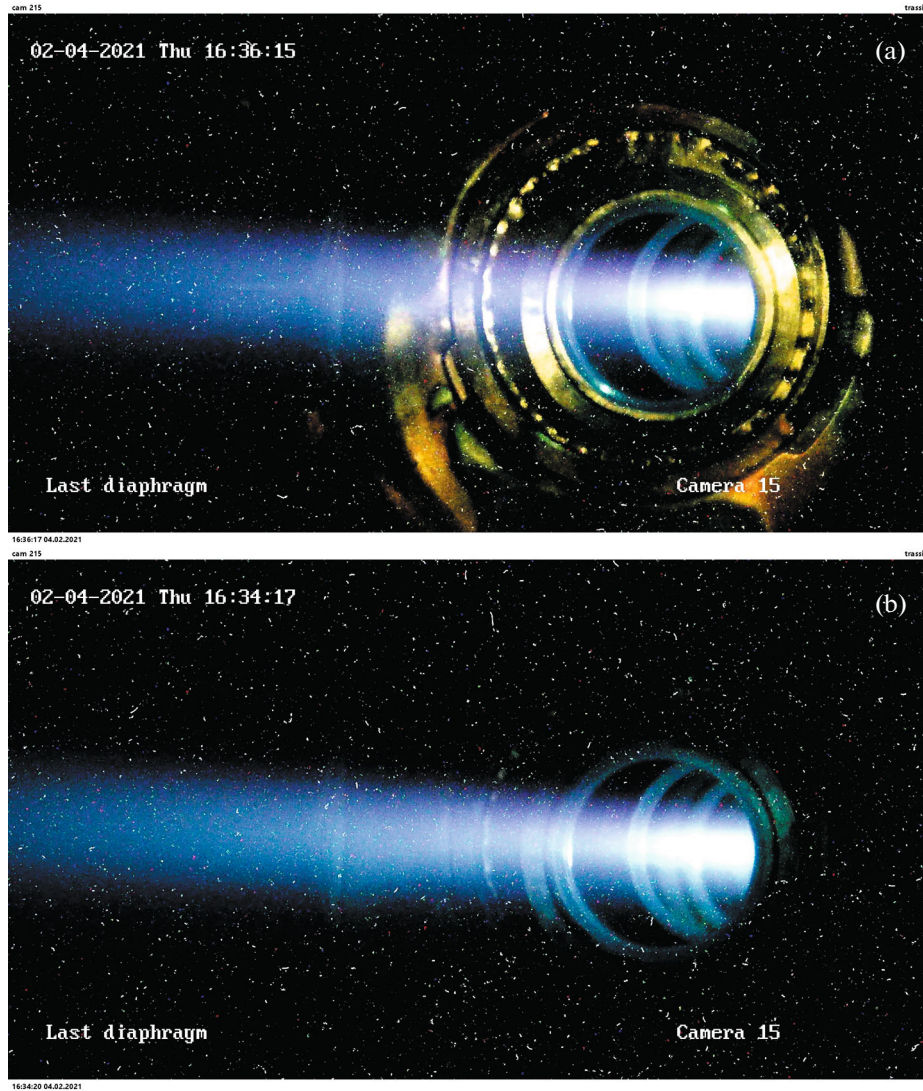


Fig. 5. Photograph of the output diaphragm of the outer electrode of the accelerator when a proton beam with a current of 3 mA is directed (a) to the center of the cooled diaphragm and (b) to a point located at a distance of 2 mm from the center.

However, since the charge density of most real beams is rarely uniform, the emittance of a real beam must be related to the fraction of particles included in the idealized beam ellipse.

Since the emittance depends on the momentum of the particles, for convenience, we use the normalized emittance ϵ_{norm} , obtained by multiplying the emittance ϵ by relativistic factors β and γ : $\epsilon_{\text{norm}} = \epsilon_{\text{rms}} \beta \gamma$, where $\beta = \sqrt{\frac{2E}{mc^2}}$ and $\gamma = \frac{1}{\sqrt{1 - \beta^2}}$, E is the energy of a charged weakly relativistic particle, and m is its mass. Thus, for protons with an energy of 2 MeV, the factors $\beta = 0.065$, $\gamma = 1.002$.

For a Gaussian beam distribution, the part of the beam included in $n\epsilon$ ellipse is determined by the

expression: $k [\%] = 100\% \times (1 - e^{-n/2})$. Thus, we get $k = 39\%$ for $n = 1$, $k = 63\%$ for $n = 2$, and $k = 86\%$ for $n = 4$. For real (non-Gaussian) beams, these values depend on the beam shape.

Let us pay attention to the fact that the emittance values given below are presented specifically for $n = 1$, although the emittance of the beam of negative hydrogen ions and the emittance of the proton beam were determined earlier from the area of the ellipse $S = 2\pi\epsilon$, whose boundary includes approximately 2/3 of the beam.

3.1. Measurement of the Phase Portrait of a Beam of Negative Hydrogen Ions Injected into the Accelerator

Using an ES-4 emittance scanner, the phase portrait of a beam of negative hydrogen ions with an

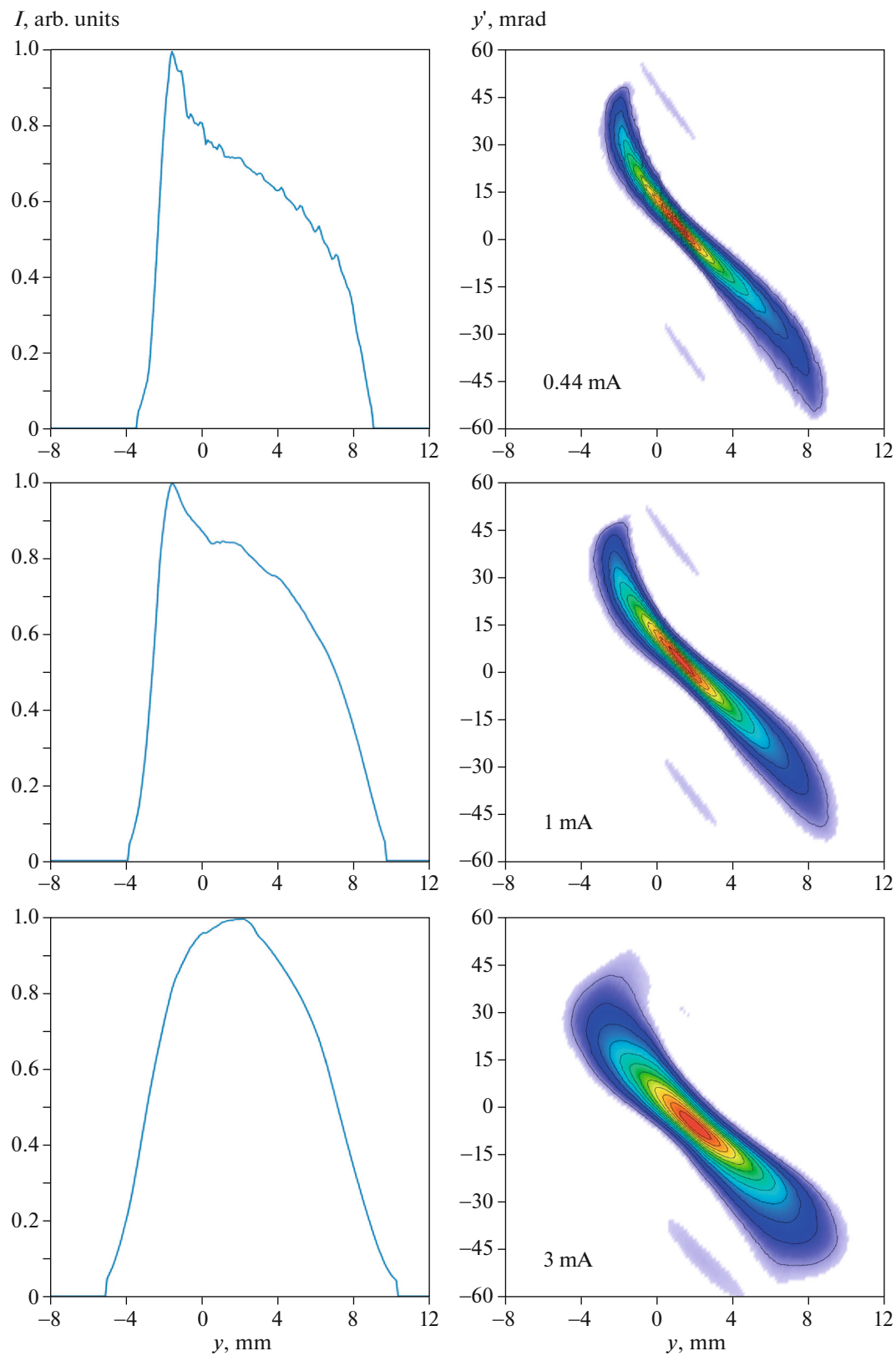


Fig. 6. Profile (left) and phase portrait (right) of the beam of negative hydrogen ions injected into the accelerator at different current values (the current values are shown in the lower left corner of the beam phase portrait).

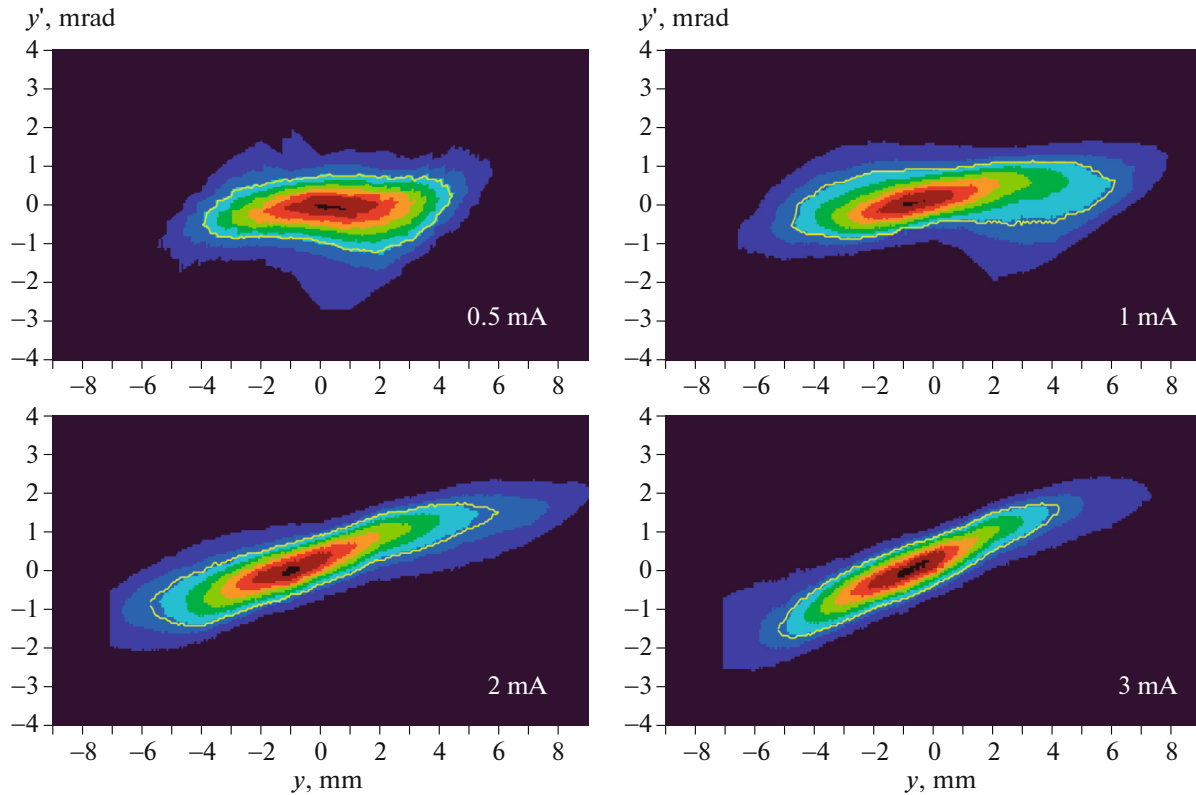


Fig. 7. Phase portrait of the proton beam (y, y') at current values of 0.5, 1, 2, and 3 mA (numbers in the lower right corner).

energy of 22 keV injected into the accelerator was measured at several current values. The measurement results are shown in Fig. 6 and in Table 1.

It can be seen that the emittance of the ion beam and the beam size increase with increasing current. The first is due to a change in the discharge in the ion source, the second is due to the action of the space charge during the transport of ions from the ion source to the accelerator.

Comparing the obtained results with those presented in [7], we conclude that the modernization of the magnetic lens made the beam more like an ellipse. The normalized ion beam emittance also decreased by 25% (from 0.27 to 0.20 mm mrad), which may be due to the optimization of ion generation.

3.2. Measurement of the Phase Portrait of a Proton Beam Obtained in an Accelerator

The phase portrait of the proton beam was measured using a cooled diaphragm scanning the beam with a step of 1 mm and an OWS-30 wire scanner measuring the profile of the proton beam that passed through the diaphragm.

Measurements of the phase portrait of the proton beam in the space of coordinates and propagation angles (x, x') and (y, y') are fulfilled at currents of 0.5,

1, 2, and 3 mA and energies of 2000 ± 2 keV. Figure 7 shows the results of measuring the phase portrait of the proton beam in space (y, y') and similar results were obtained in the space (x, x'). Table 2 shows the characteristics of the ellipse and emittance of the proton beam phase portrait.

Let us discuss the phase portrait of the proton beam by analyzing Fig. 7 and Table 2. Figure 7 shows how the portrait changes with increasing current. If, at a current of 0.5 mA, the beam is practically parallel and has a transverse dimension $y = 4.2$ mm, then its size increases and it becomes divergent with increasing current. Thus, at a current of 3 mA, the beam is characterized by a divergence $y' = 1.6$ mrad and has a transverse dimension $y = 5.2$ mm. This behavior is

Table 2. Results of measurements of the phase portrait of the proton beam

Current, mA	y , mm	y' , mrad	ϵ_{norm} , mm mrad
0.5	4.2	0.38	0.21
1	5.6	0.56	0.27
2	6.1	1.2	0.24
3	5.2	1.6	0.21

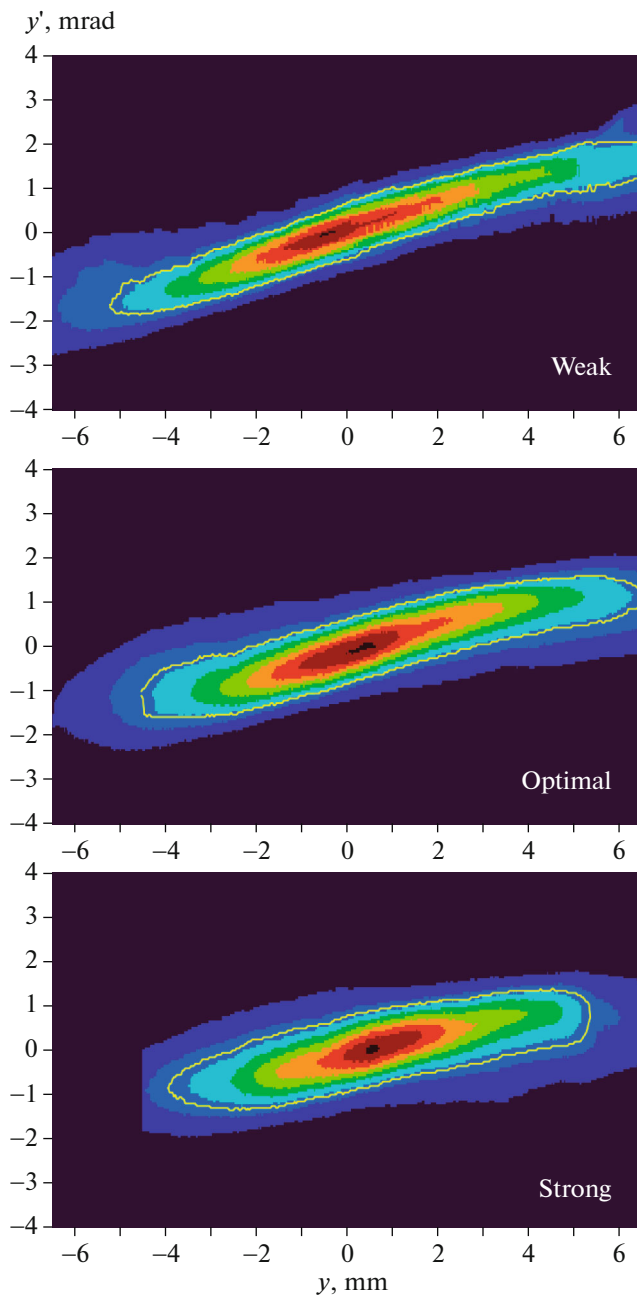


Fig. 8. Phase portrait of a proton beam with a current of 2 mA for weak, optimal, and strong magnetic lens focusing modes.

explained by the action of the space charge in the transport path of the negative hydrogen ion beam: as the current increases, the action of the space charge increases, the ions acquire an additional transverse momentum, and the beam becomes wider.

Let us pay attention to the fact that at intermediate current values, 1 and 2 mA, the proton beam is wider and its emittance is larger. This is due to the fact that the beam of negative hydrogen ions is introduced in

Table 3. Results of measurements of the phase portrait of a proton beam with a change in the focusing mode.

Focus mode	y , mm	Y' , mrad	ϵ_{norm} , mm mrad
Weak	6.0	1.7	0.20
Optimal	5.4	1.2	0.22
Strong	4.6	0.9	0.21

this case into the accelerator not along the axis but slightly above or below, and the strong input electrostatic lens of the accelerator splits the ion beam. This effect is especially noticeable in Fig. 7 at a current of 1 mA: the ellipse seems to be pulled in the middle. It is for this reason that special attention is paid to controlling the position of the ion beam using a wire scanner in the normal mode during the injection of a beam of negative hydrogen ions into the accelerator. In this case, a wire scanner was used to measure the phase portrait of the proton beam, and the position of the negative hydrogen ion beam was not controlled by it.

Let us also pay attention to the fact that, at a current of 3 mA, the normalized emittance of the injected beam of negative hydrogen ions is practically equal to the emittance of the proton beam. This behavior at a current of 3 mA is explained by the fact that the mode of operation at this current is often used and is optimized.

Since the space charge does not affect the transport of the proton beam [11], let us estimate the size of the proton beam on the surface of the lithium target, which is planned to be installed in a neighboring bunker at a distance of 10.7 m from the center of the accelerator. For an upper estimate, consider the most divergent beam obtained at 3 mA. At a distance of 1.86 m from the center of the accelerator, the beam size $y = 5.2$ mm and divergence $y' = 1.6$ mrad. This means that the beam size will be 19 mm at a distance of 10.7 m from the center of the accelerator. This size is less than the radius of the lithium target, which is equal to 50 mm; therefore, the proton beam can be transported to the target without the use of additional focusing elements.

Let us now study the influence of the strength of the magnetic lens on the proton beam. Let us measure the phase portrait of the proton beam at the standard magnetic lens strength (we call this mode “optimal”) as well as at a decrease or increase in the current in the lens coils by 1.6% (we call these modes “weak” and “strong,” respectively). Figure 8 shows the results of measuring the phase portrait of the proton beam at a current of 2 mA and Table 3 shows its characteristics.

As can be seen, when the focusing regime changes from weak to strong, both the beam size and its angular

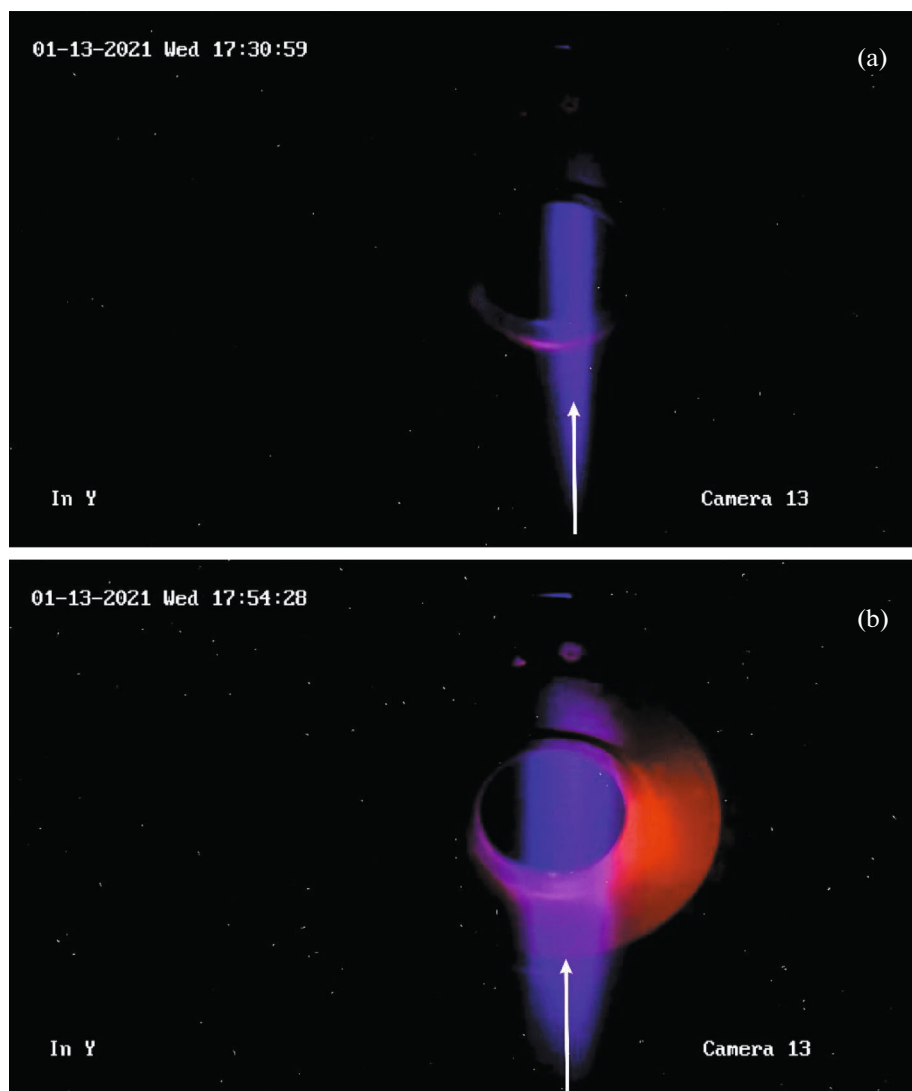


Fig. 9. Image of the input diaphragm of the external accelerating electrode in the (a) optimal and (b) strong focus modes. The arrow points to the accelerated beam of negative hydrogen ions.

divergence decrease. It seems that strong focus mode is better than optimal. However, as seen in Fig. 9, in the strong focusing mode, the input aperture of the external accelerating electrode heats up to a level unsuitable for continuous operation.

3.3. Measurement of the Phase Portrait of the Accompanying Flux of Neutrals

Such a flow of argon is usually injected into the gas-stripping target of the accelerator to ensure the recharging of 95% of negative ions into positive ones. This means that the resulting proton beam is accompanied by a stream of neutrals with an equivalent current of 5% of the proton beam current.

Let us measure the phase portrait of the accompanying neutral flux as follows. Firstly, we deflect the

proton beam down with a bending magnet. Secondly, we will apply positive rather than negative voltage to the metal rings installed near the wire scanner. This will make it possible to extract secondary electrons knocked out from the scanner wire under the action of neutrals with an energy of 1 MeV and to measure the current of neutrals. Of course, the value of this current is less than the current of protons, but it is quite sufficient for constructing a phase portrait of the neutral flux. Examples of the phase portrait of the accompanying neutral flux for a proton beam with an energy of 2 MeV and a current of 2 mA are shown in Fig. 10.

It was determined that the size of the neutral flux is 6–6.5 mm and its divergence is 1.9–2.4 mrad. It can be seen that the size and divergence of the neutral flux is greater than the size and divergence of the proton beam. The point is that a flux of neutrals with an

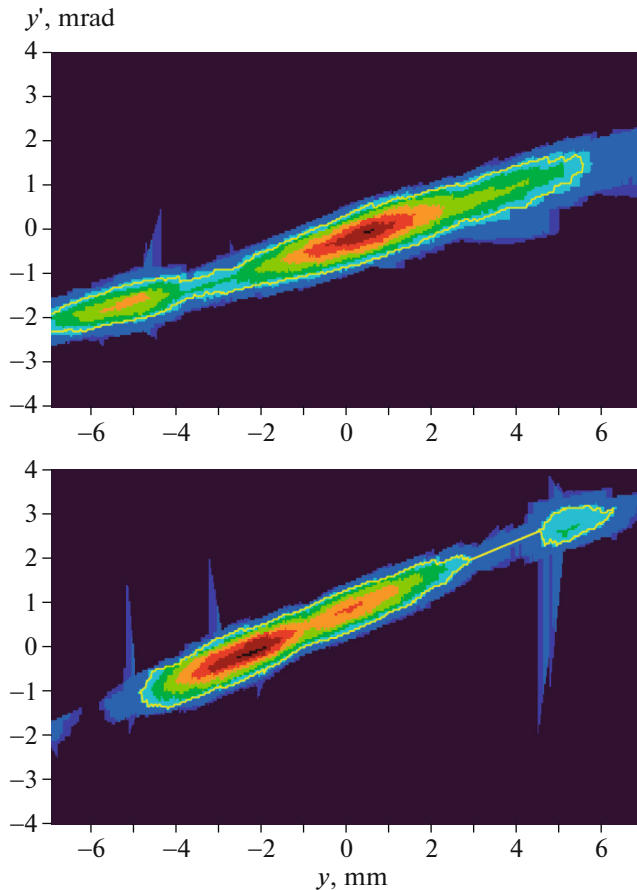


Fig. 10. Phase portraits of the neutral flux at a current of 2 mA of a 2 MeV proton beam in different focusing modes.

energy of 1 MeV is formed in the gas-stripping target of the accelerator from 1-MeV negative hydrogen ions, which have lost only one electron during stripping. Most of the negative hydrogen ions lose both electrons and form a beam of protons with an energy of 1 MeV. Inside a gas-stripping target, the phase portraits of a 1 MeV neutral flux and a 1 MeV proton beam should be similar. However, if the neutrals propagate further in a straight line, then the electric field acts on the protons, accelerating them in the longitudinal direction, focusing in the region of the diaphragm of the high-voltage electrode and defocusing in the region of the accelerator outlet. The action of the electric field explains the difference between the phase portraits of the neutral flux and the proton beam.

Since neutrals propagate rectilinearly, knowing the characteristics of the neutral flux at a distance of 1.86 m from the center of the accelerator, we can estimate the size of the neutral flux inside the gas-stripping target located at the center of the accelerator. We obtain that the size of the neutral flux in the stripping target is 2–2.5 mm. The size of the ion beam in

the stripping target should be the same. The obtained value is in good agreement with the size of the glow with a radius of 2 mm, recorded by the Celestron Ultima 80-45 long-focus telescope, installed instead of a lithium target (10 in Fig. 1) and directed through a cooled copper mirror to a gas-stripping target along its axis. Figure 11 shows the image taken by the telescope.

CONCLUSIONS

The tandem electrostatic accelerator with vacuum insulation described in the paper is characterized by an original design and is intended for the development of boron neutron capture therapy and a number of other applications.

The phase portrait of the ion beam was measured in three places: at the entrance to the accelerator, inside the stripping target of the accelerator, and at the exit from the accelerator. The dependence of the beam on the ion current and on the strength of the magnetic lens focusing the beam of negative hydrogen ions at the entrance to the accelerator is studied.

The following has been established.

1. Modernization of the magnetic lens, which focuses the beam of negative hydrogen ions at the entrance to the accelerator, reduced the spherical aberration of the lens.

2. With an increase in the current of negative hydrogen ions drawn from the ion source, the emittance of the ion beam increases: from $\epsilon_{\text{norm}} = 0.13$ mm mrad at 0.44 mA to $\epsilon_{\text{norm}} = 0.20$ mm mrad at 3 mA.

3. With an increase in the current of negative hydrogen ions, the transverse size of the ion beam injected into the accelerator increases due to the action of the space charge during the transport of ions from the ion source to the accelerator. It is shown that the effect of the space charge on the subsequent ion acceleration can be compensated by changing the strength of the magnetic lens focusing the ion beam at the accelerator input.

4. Inside the gas-stripping target, the ion beam has a diameter of 4 mm and its divergence is ± 2 mrad.

5. At the output of the accelerator, the optimally focused proton beam has a diameter of 10 ± 1 mm, a divergence of ± 1.5 mrad, and an emittance $\epsilon_{\text{norm}} = 0.2$ mm mrad. Such a beam can be delivered to a distance of 10.7 m to a lithium target 100 mm in diameter without the use of additional focusing elements.

FUNDING

The study was supported by a grant from the Russian Science Foundation (project no. 19-72-30005). The

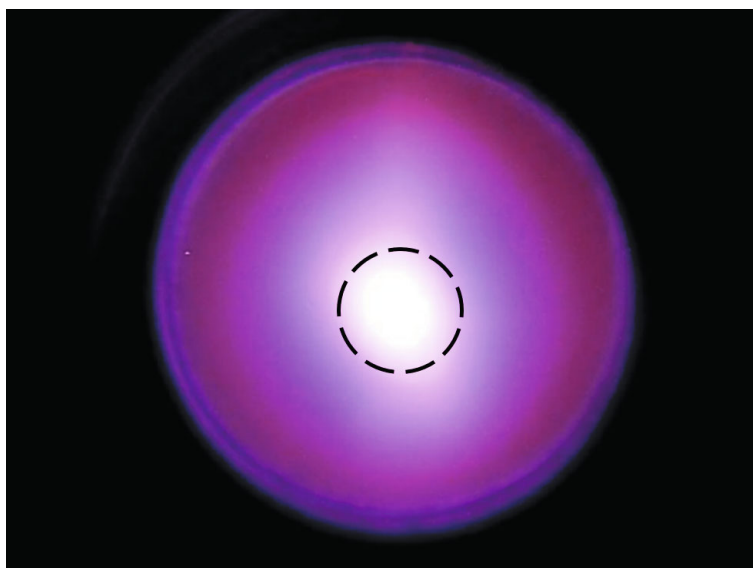


Fig. 11. Image from a video camera connected to a telescope looking through a copper cooled mirror at a gas-stripping target. The dashed line denotes the diameter of 5 mm, the diameter of the stripping target tube is 16 mm.

authors thank D-Pace (Canada) for the well-made wire scanner and emittance scanner used in this study.

REFERENCES

1. Taskaev, S., Berendeev, E., Bikchurina, M., Bykov, T., Kasatov, D., Kolesnikov, I., Koshkarev, A., Makarov, A., Ostreynov, G., Porosev, V., Savinov, S., Shchudlo, I., Sokolova, E., Sorokin, I., Sycheva, T., and Verkhovod, G., *Biology*, 2021, vol. 10, no. 5, p. 350. <https://doi.org/10.3390/biology10050350>
2. Dymova, M., Dmitrieva, M., Kuligina, E., Richter, V., Savinov, S., Shchudlo, I., Sycheva, T., Taskaeva, I., and Taskaev, S., *Radiat. Res.*, 2021, vol. 196, no. 2, p. 192. <https://doi.org/10.1667/RADE-21-00015.1>
3. Badrutdinov, A., Bykov, T., Gromilov, S., Higashi, Y., Kasatov, D., Kolesnikov, I., Koshkarev, A., Makarov, A., Miyazawa, T., Shchudlo, I., Sokolova, E., Sugawara, H., and Taskaev, S., *Metals*, 2017, vol. 7, no. 12, p. 558. <https://doi.org/10.3390/met7120558>
4. Bykov, T., Goloshevskii, N., Gromilov, S., Kasatov, D., Kolesnikov, I., Koshkarev, A., Makarov, A., Ruktuev, A., Shchudlo, I., Sokolova, E., and Taskaev, S., *Nucl. Instrum. Methods Phys. Res., Sect. B*, 2020, vol. 481, p. 62. <https://doi.org/10.1016/j.nimb.2020.08.010>
5. Shoshin, A., Burdakov, A., Ivantsivskiy, M., Polosatkin, S., Semenov, A., Sulyaev, Yu., Zaitsev, E., Polozova, P., Taskaev, S., Kasatov, D., Shchudlo, I., and Bikchurina, M., *Fusion Eng. Des.*, 2021, vol. 168, p. 112426. <https://doi.org/10.1016/j.fusengdes.2021.112426>
6. Taskaev, S., Bykov, T., Kasatov, D., Kolesnikov, I., Koshkarev, A., Makarov, A., Savinov, S., Shchudlo, I., and Sokolova, E., *Nucl. Instrum. Methods Phys. Res., Sect. B*, 2021, vol. 502, p. 85. <https://doi.org/10.1016/j.nimb.2021.06.010>
7. Bykov, T.A., Kasatov, D.A., Kolesnikov, I.A., Koshkarev, A.M., Makarov, A.N., Ostreynov, Yu.M., Sokolova, E.O., Sorokin, I.N., Taskaev, S.Yu., and Shchudlo, I.M., *Instrum. Exp. Tech.*, 2018, vol. 61, no. 5, p. 713. <https://doi.org/10.1134/S0020441218050159>
8. <https://www.d-pace.com/?e=70>.
9. <https://www.d-pace.com/?e=2>.
10. Makarov, A.N., Sokolova, E.O., and Taskaev, S.Yu., *Instrum. Exp. Tech.*, 2021, vol. 64, no. 1, p. 24. <https://doi.org/10.1134/S0020441220060184>
11. Bykov, T.A., Kasatov, D.A., Kolesnikov, I.A., Koshkarev, A.M., Makarov, A.N., Ostreynov, Yu.M., Sokolova, E.O., Taskaev, S.Yu., and Shchudlo, I.M., *Tech. Phys.* 2021, vol. 66, no. 1, p. 98. <https://doi.org/10.1134/S1063784221010047>